Studies of Dust Transport in Long Pulse Plasma Discharges in the Large Helical Device

M Shoji[1], H Kasahara[1], M Tokitani[1], T Seki[1], K Saito[1], S Kamio[1], R Seki[1], Y Tanaka[2], A Pigarov[3], R Smirnov[3], G Kawamura[1], H Tanaka[1], S Masuzaki[1], Y Uesugi[2], T Mutoh[1] and LHD Experiment Group[1]

[1]National Institute for Fusion Science, 322-6 Oroshi-cho, Toki 509-5292, Japan

[2]Kanazawa University, Kakuma, Kanazawa 920-1192, Japan

[3]University of California at San Diego, La Jolla, CA92093, USA

E-mail: shohji.mamoru@nifs.ac.jp

Abstract. The three-dimensional trajectories of incandescent dusts in plasmas was observed with stereoscopic fast framing cameras in the large helical device. It proved that the dusts locate in the peripheral plasma and the most of the dusts move along the magnetic field lines with acceleration which direction corresponds to the plasma flow. ICRF heated long pulse plasma discharges were terminated with release of large amounts of dusts from a closed divertor region. After the experimental campaign, the traces of exfoliation of carbon rich mixed-material deposition layers were found in the divertor region. Transport of carbon dusts is investigated using a modified dust transport simulation code which can explain the observed dust trajectories. It also shows that control of the radius of the dusts to less than 1mm is necessary to prevent the plasma termination by penetration of dusts for the long pulse discharges. Dust transport simulation including heavy metal dusts demonstrates that high heating power operation is effective for shielding the main plasma from the dust penetration by an enhanced plasma flow effect and a high heat load onto the dusts in the peripheral plasma. It shows more powerful penetration characteristic of tungsten dusts compared to that of carbon and iron dusts.

1. Introduction

Dusts in plasma confinement devices have recently gained attention from the viewpoint of the influence on the main plasma performances [1-5]. It has been believed that the thick layers of eroded materials from divertor plates and the vacuum vessel, which are deposited on divertor regions, are break up into dusts. It has been concerned that large amounts of impurities included in the dusts penetrate into the main plasma and induces radiation collapses or plasma disruptions and so on. The radioactivity and the chemical activity of dusts can also be a major concern in the case of serious vacuum accidents in future nuclear fusion reactors [6, 7]. Long pulse plasma discharge experiments in the Large Helical Device (LHD) provide unique opportunities for studying physical processes of formation of dusts due to plasma-wall interactions under saturated wall conditions (no wall pumping) which are equivalent to those in nuclear fusion reactors. It is experimentally found that mixed-material deposition layers are accumulated and deposited on the surface of the vacuum vessels and divertor regions, which can lead to release of large amounts of dusts caused by exfoliation of the deposition layers induced by interaction with the peripheral plasma and the thermal stresses on the layers, etc.

On the influences of dusts on the main plasma, the following two experimental results were observed in long pulse discharge experiments in the LHD.

- *Release of iron dusts with sparks in past ICRF heated long pulse discharges*

In past ICRF heated long pulse discharges in 2004-2006, termination of the plasma discharges by release of dusts from the inboard side of the tours was observed with a tangentially viewing CCD camera, which is synchronized with sparks in the vacuum vessel in the inboard side of the torus. Abrupt increase in emission of iron ions was detected just before the plasma termination. It is possible that the penetration of iron dusts into the main plasma caused the termination of the plasma discharges by radiation collapse [8].

- *Release of large amounts of carbon dusts in long pulse discharges in the last experimental campaign*

Plasma termination was observed in ICRF heated long pulse discharges in the last experimental campaign in 2013. Release of large amounts of dusts from a toroidal edge of a closed divertor installed in the inboard side of the torus near a lower port was observed with sparks at the end of the long pulse discharges. It is found that the plasma termination is synchronized with abrupt increase in emission of carbon ions (CIII) [9].

The above two observations strongly motivated us to study dust transport in LHD plasmas for sustaining and achieving high performance plasmas in steady state operation. In this paper, an experimental setup for observing dust transport is explained in the next section. Observations of the three-dimensional trajectories of dusts and release of dusts in long pulse discharges are presented in section 3 and 4, respectively. Analyses using a modified dust transport simulation code for long pulse plasma discharges are shown in section 5. The effect of high plasma heating power operation on transport of heavy metal dusts such as iron and tungsten is investigated in section 6. A summary is described in the last section.

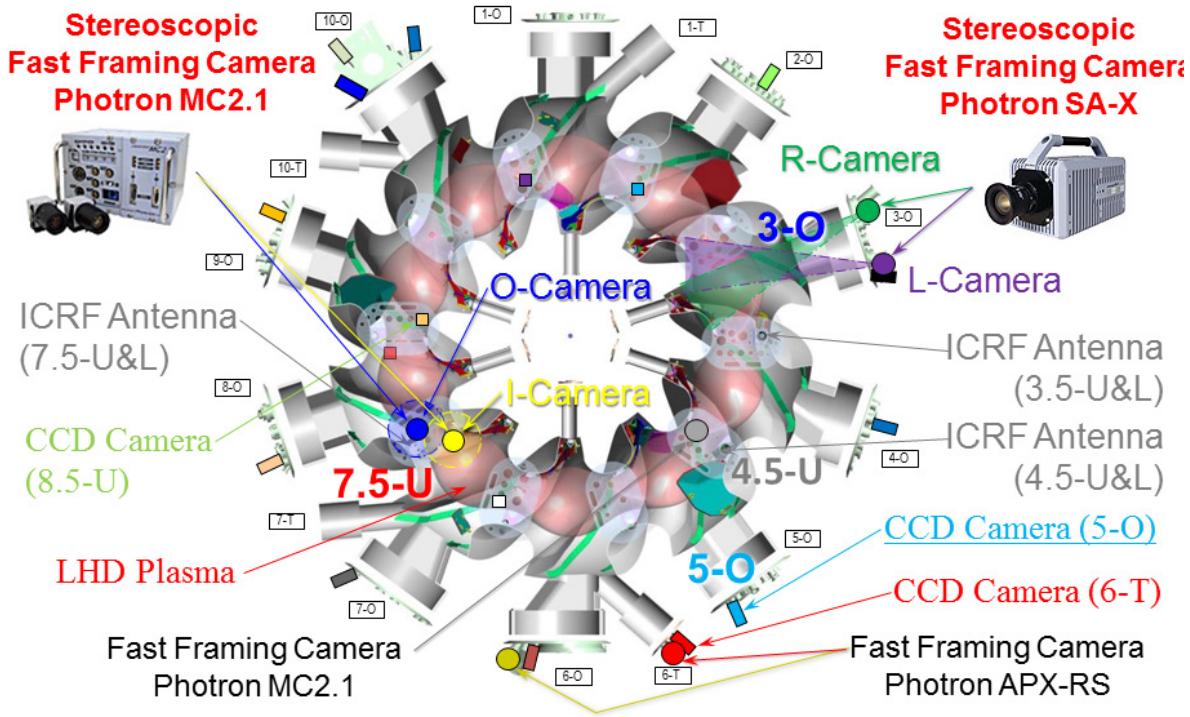

Figure 1. Top view of the experimental setup of plasma heating systems (ICRF antennas), visible CCD cameras (colored squares) and visible C-MOS fast framing cameras (colored circles) for monitoring LHD plasmas and plasma wall interactions in long pulse plasma discharges.

2. Experimental setup for observing transport of dusts in LHD plasmas

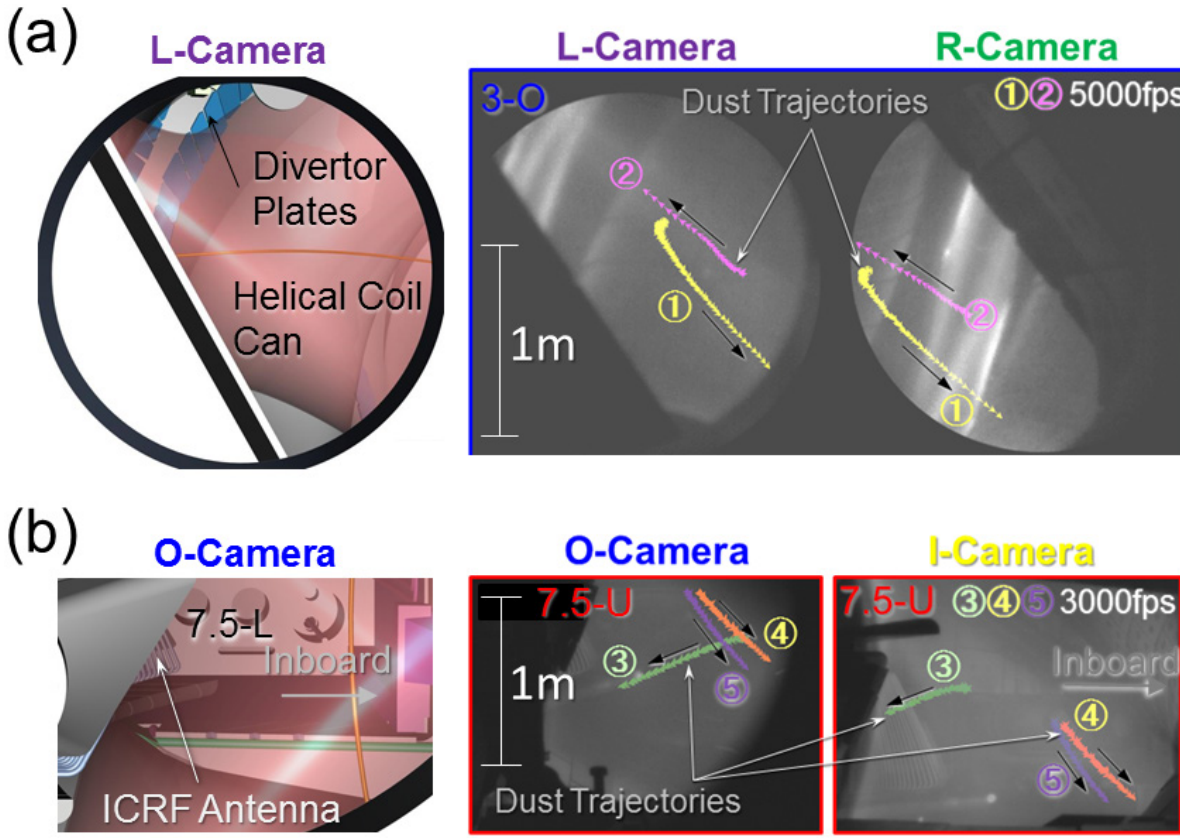

Figure 2. Stereoscopic views of a LHD plasma taken with stereoscopic fast framing cameras installed in 3-O (a) and 7.5-U ports (b), respectively, with CAD images viewed from a position of the lenses for the cameras (left images). The trajectories of incandescent dusts on the images are indicated as small colored triangles which are plotted at regular time intervals.

The LHD is the largest helical device in the world with superconducting helical and poloidal coils, providing current-less long pulse plasma discharge operation [10]. One of the features of LHD plasmas is the three-dimensionally complicated structure of the peripheral plasma. An ergodized magnetic field lines are formed in the outside of the Last Closed Flux Surface (LCFS) which is called as 'ergodic layer', and four bundle magnetic field lines (divertor legs) are deviated from two X-points in the ergodic layer. The magnetic field lines in the divertor legs and the ergodic layer are directly connected to the vacuum vessel (stainless steel) and divertor plates (carbon) which are installed along two helically distributed strike points in the vacuum vessel. For the original open divertor configuration, the front side of the divertor plates was faced to the main plasma. Long pulse plasma discharges are sustained by ion cyclotron range of frequency (ICRF) with electron cyclotron resonance heating (ECRH) in a hydrogen minority heating regime. For plasma heating in long pulse discharges by ICRF, totally three types of ICRF antennas are mounted at three different toridal posistions (see figure 1).

In order to monitor LHD plasmas and plasma-wall interactions in the vacuum vessel in long pulse discharges, about thirty visible CCD cameras and three visible fast framing C-MOS cameras have been installed in various toroidal/poloidal positions as shown in figure 1. The CCD cameras can acquire images at a rate of 30fps (frames per second). The fast framing cameras, which are installed in outer ports (3-O and 6-O), upper ports (7.5-U and 4.5-U) and a tangential port (6-T) have a function to take images at rates of more than 3,000fps. The fast framing cameras installed in 7.5-U and 3-O ports are equipped with two separated image sensor heads and stereo optics, respectively. It can

simultaneously capture two images viewed from two different positons, providing stereoscopic observation of three-dimensional dust trajectories. Some fiducial points were set on the surface of vacuum components in the viewing area of the stereoscopic fast framing cameras in order to know the exact spatial configuration of the cameras, which is for accurate observation of dust trajectories.

3. Observations of three-dimensional dust trajectories by stereoscopic measurement

Three-dimensional dust trajectories have been observed with the two stereoscopic fast framing cameras for a standard magnetic configuration (the radial position of the magnetic axis R_{ax}=3.60m). The trajectories of dusts are identified as traces of incandescent moving spots in images taken with the cameras because dusts entering the peripheral plasma are heated up and emit visible light by heat load onto the dusts in the plasma. Figure 2 (a) and (b) are stereoscopic views of a LHD plasma taken with the fast framing cameras installed in 3-O and 7.5-U ports, respectively, in which some typical observed incandescent dust trajectories are indicated as series of small colored triangles which are plotted at regular time intervals. It presents that the most of dusts pass through the observation areas of the stereoscopic cameras with acceleration. The three-dimensional dust trajectories are derived from the analyses of the positions of the incandescent spots on the stereoscopic images using a pinhole camera model. This model requires a 'camera matrix' which is for transforming points on two-dimensional coordinates on the image sensor in the camera to real three-dimensional coordinates. In order to obtain the 'camera matrix', spatial calibration of the stereoscopic cameras was carried out after the experimental campaigns by reproducing the spatial configuration of the cameras in a laboratory using the information of the three-

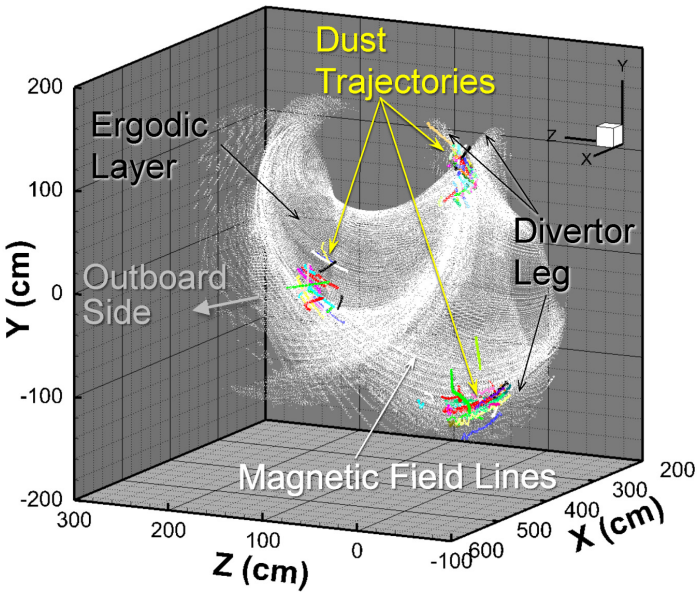

Figure 3. Perspective view of the three-dimensional trajectories of dusts (colored dotted lines) observed with stereoscopic fast framing cameras installed in an outer port (3-O) and an upper port (7.5-U) with plots of magnetic field lines in the peripheral plasma (small white dots). The positions of the dust trajectories in the two different toroidal positions are combined into one toroidal section.

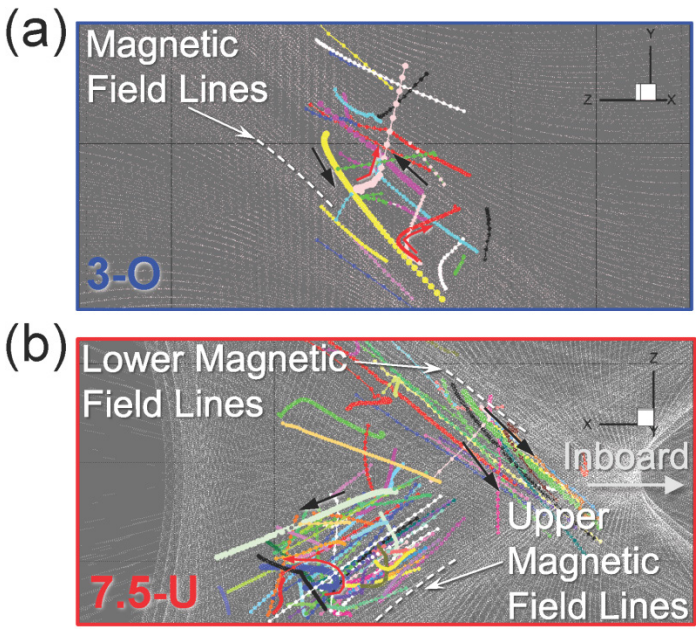

Figure 4. Enlarged images of the observed three-dimensional dust trajectories (colored dotted lines) viewed from an outer port (3-O) (a), and those from an upper port (7.5-U) (b) with plots of magnetic field lines in the peripheral plasma (small white dots). Representative magnetic field lines in the outboard side and lower/upper divertor legs are highlighted by broken white lines.

dimensional positions of the fiducial points located in the viewing areas of the cameras. The coordinates of the dust positions on the stereoscopic images are traced frame by frame using an image processing software. The dust positions on the images are regarded as the center of the incandescent spots which intensity is more than a threshold value after the subtraction of the background intensity profiles in the viewing areas.

Figure 3 is a perspective view of the three-dimensional trajectories of the dusts observed with the two stereoscopic fast framing cameras installed in 3-O and 7.5-U ports. Colored dotted lines indicate the overlaid dust trajectories in some different plasma discharges and times. Small white dots mean the magnetic field lines in the LHD peripheral plasma. It shows that the positions of the dust trajectories locate at the outer edge of the ergodic layer and in the lower/upper divertor legs, indicating that the peripheral plasma have a function for protecting the main plasma from the penetration of dusts released from the outside of the main plasma. It is probable that the dusts are heated and finally sublimated or evaporated by the heat load onto the dusts in the peripheral plasma.

Figure 4 (a) and (b) show enlarged images of the observed dust trajectories viewed from the outer and the upper ports, respectively, in which the direction of movement of the typical observed incandescent dust trajectories shown in figure 2 are indicated by small black arrows. The direction of the movement of the dusts can be explained by the spatial distribution of the plasma flow velocity in the LHD peripheral plasma [11]. All dust trajectories shown in figure 4 (a) locate in the outer edge of the ergodic layer in the outboard side of the torus. In figure 4 (b), groups of dust trajectories near the right-upper and the left-lower corners correspond to dusts moving along the magnetic field lines in the lower and upper divertor legs, respectively. The figures present that the most of the observed dusts move along the magnetic field lines in the ergodic layer and the lower/upper divertor legs which are indicated as broken white lines. It also shows that while the most of dust trajectories are almost straight along the magnetic field lines, there are some unusual dusts which have sharply curved trajectories crossing the magnetic field lines which are indicated by small red arrows as some examples in the figures.

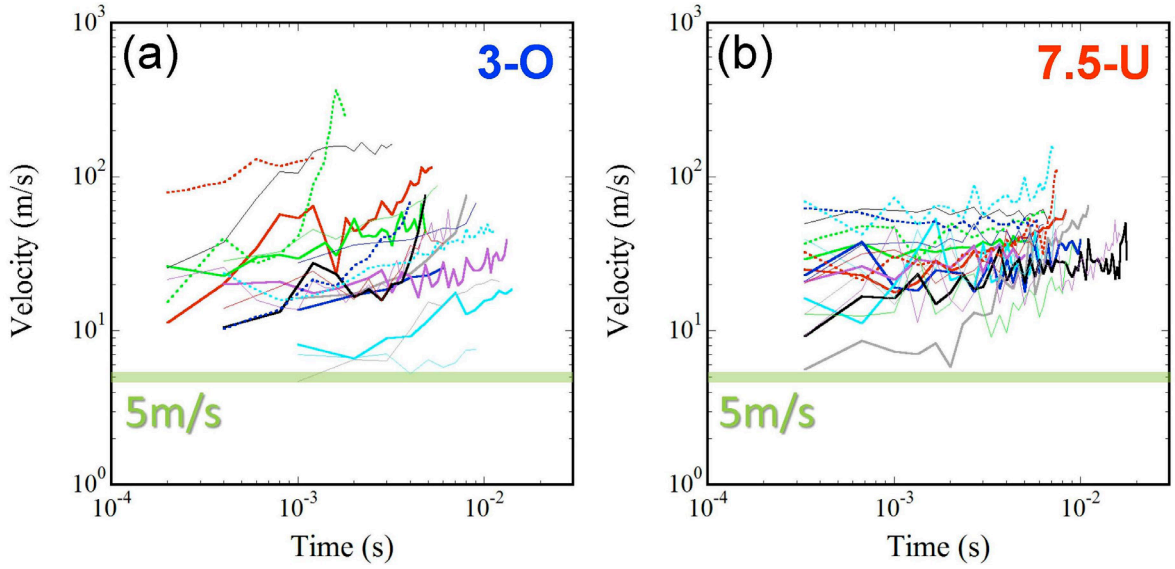

Figure 5. Time evolution of representative dusts velocities observed with stereoscopic fast framing cameras installed in an outer port (3-O) (a) and an upper port (7.5-U) (b). The velocities of most of dusts increase with time. A typical initial velocity of dusts is estimated from the lower envelope of the time evolution to be about 5m/s.

The moving velocities of the observed dusts can be obtained from the coordinates of the dust positions on the trajectories and the framerate of the fast cameras at the observations. Figure 5 (a) and (b) give the time evolution of observed dust velocities on the elapsed time after the dusts appeared on the stereoscopic images viewed from the 3-O and 7.5-U ports, respectively. Observations of some unusual dusts, which have sharply curved trajectories, are also included in the time evolution of the

dust velocities in the figures. It shows that the most of the dusts move with acceleration in the latter half of the time evolution. It is probable that the observed dusts have received the effect of the plasma flow in the peripheral plasma. The following dust transport simulation analysis presented in section 5 shows that acceleration of dust movement strongly depends on the dust sizes (weight). In other words, small sized (light weighted) dusts can be easily accelerated by the effect of the plasma flow due to the small inertial mass compared to that of large sized (heavy weighted) dusts. Because it is probable that the most of the observed dusts went into the viewing area of the stereoscopic fast cameras after receiving the effect of the plasma flow, an initial dust velocity corresponding to that at the dust release points can be approximately estimated from the lower envelope of the time evolution of the observed dust velocities, which gives an initial dust velocity of about 5m/s.

4. Release of dusts in ICRF heated long pulse plasma discharges in the last experimental campaign

In a series of the experimental campaigns, the termination process in ICRF heated long pulse discharges has historically changed according to increase in the plasma heating power, optimization of the gas fueling technique, change of the divertor configuration, etc. Past long pulse plasma discharges in 2004-2006 were often terminated with release of iron dusts from the surface of the vacuum vessel in the inboard side of the torus [8]. The plasmas were sustained by ICRF (PA antenna in 7.5-U&L ports) with a relatively low heating power of ~0.5MW and a low plasma density of $\sim 0.4\times10^{19}m^{-3}$ for about 54 minutes [12]. From the experimental campaign in 2010, the plasma heating system was improved and an additional ICRF antenna (HAS antenna) was introduced to 3.5-U&L ports. It enabled sustainment of plasma discharges with a higher total heating power of ~1MW and a higher plasma density of $\sim 1.1\times10^{19}m^{-3}$. It successfully contributed to sustainment of long pulse discharges having resistance to the release of dusts. As a result, termination of the plasma discharges with release of iron dusts was significantly reduced, and the reason for termination of the discharges changed to the stop of the ICRF power in the experimental campaigns after 2010. The plasma heating power was stopped by a reflection interlock and detection of breakdown in the antennas, which was synchronized with sparks in the antennas and the abrupt increase in the emission of iron ions in the plasmas (FeXVI) [13]. It

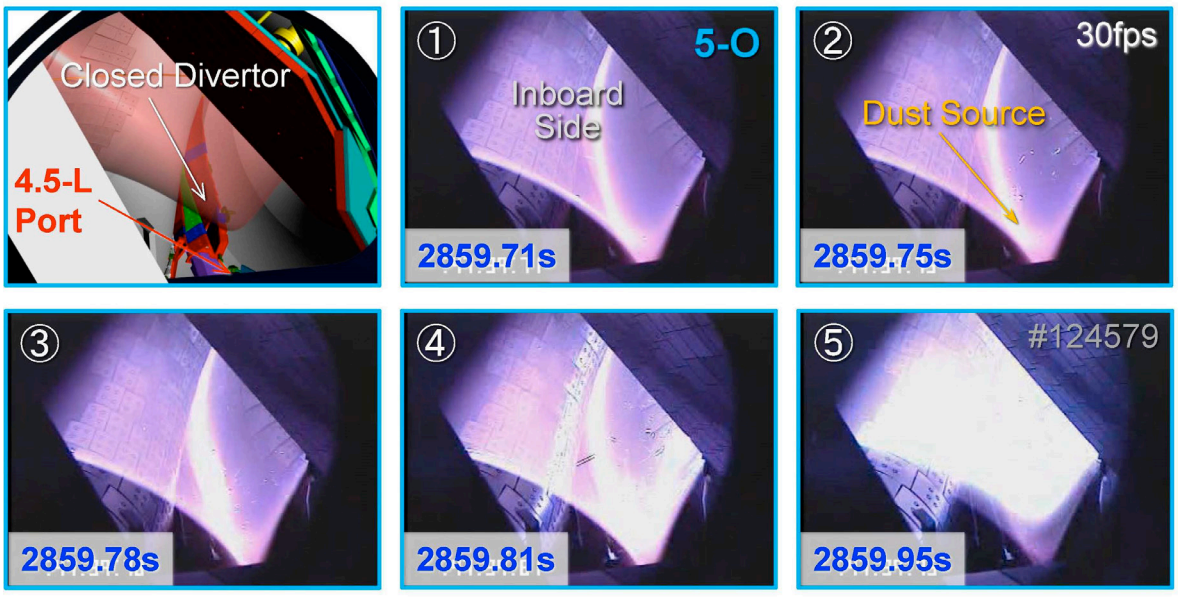

Figure 6. Sequential images taken with a CCD camera installed in an outer port (5-O) just before termination of a long pulse discharge in the last experimental campaign in 2013. The upper-left image is a CAD image viewed from the camera position, which shows a closed divertor configuration at a toroidal edge in the inboard side of the torus near a lower port (4.5-L).

could be caused by release of iron-rich dusts from the antennas, which is composed of stainless steel, due to physical sputtering in the antennas.

In the last experimental campaign in 2013, an ICRF antenna (FAIT antenna) was newly introduced to 4.5-U&L ports [14]. Some improvements for preventing electric breakdown, such as tungsten coating on the surface of the antenna strips, and removal of a part of Faraday shields and so on, were applied to the existing ICRF antennas, and the most of the divertor configuration was changed from the original open divertor configuration to closed one in which the front side of the divertor plates directly face to the inboard side of the torus with triangularly roof shaped dome structures to effectively confine neutral particles in the divertor region [15]. In the last experimental campaign, a plasma discharge was successfully sustained for about 47 minutes with a higher heating power of ~1.2MW and a higher plasma density of $\sim 1.2\times10^{19}m^{-3}$. The long pulse discharges have mostly been interrupted with release of large amounts of dusts released from the closed divertor regions near lower and upper ports.

A CCD camera installed in an outer port (5-O) and a fast framing camera in an upper port (4.5-U) observed the release of dusts just before the termination of a long pulse discharge. Figure 6 gives the sequential images taken with the CCD camera (5-O) just before the plasma termination with a CAD image viewed from the position of the camera, which shows a closed divertor configuration at a toroidal edge near a lower port (4.5-L) in the inboard side of the torus. In the closed divertor configuration, some divertor plates are installed so as to directly intersect a peripheral plasma on a divertor leg for changing the strike points to the inboard side in order to efficiently confine neutral particles in the divertor region. Figure 6 looks that the plasma termination occurred synchronized with the release of large amounts of incandescent dusts from the closed divertor region in the inboard side of the torus near the lower port (4.5-L) with sparks.

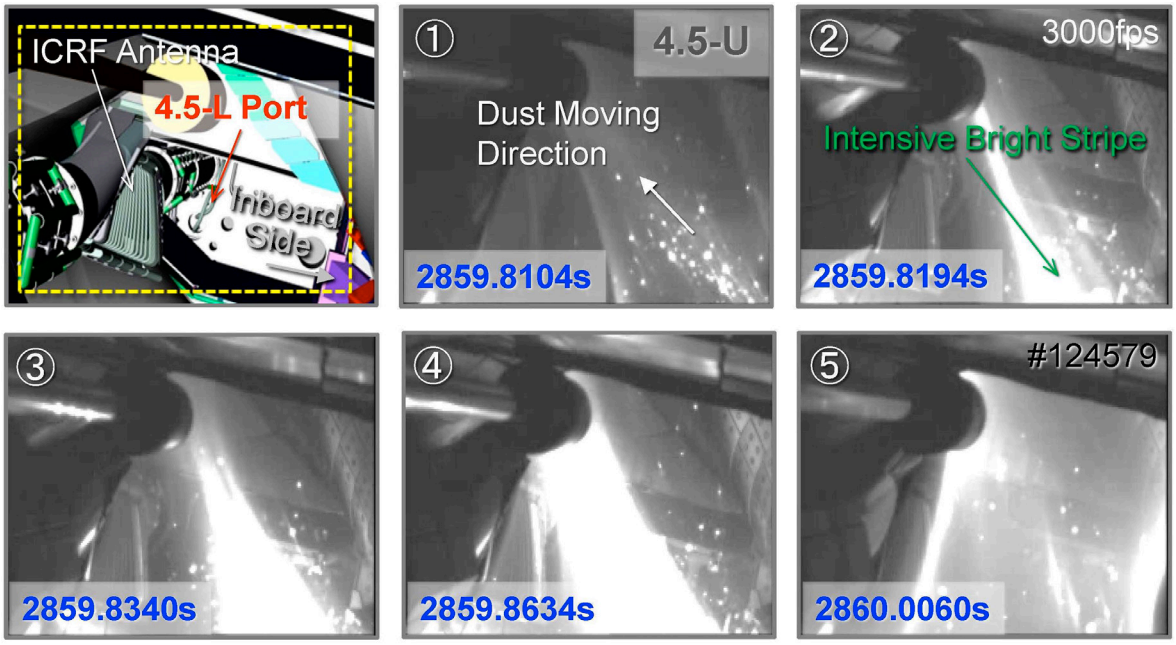

Figure 7. Sequential images of a long pulse discharge just before the plasma termination, which taken with a fast framing camera installed in an upper port (4.5-U). The upper-left image is a CAD image viewed from the camera position. Right-lower corner in the images corresponds to the closed divertor region installed in the inboard side of the torus near a lower port (4.5-L). The moving direction of observed dusts is indicated as a white arrow in the first frame (the upper-middle image).

A fast framing camera, which was not a stereoscopic one, was mounted in an upper port (4.5-U) in the long pulse discharge. Figure 7 displays sequential images taken with the fast framing camera which show that the large amounts of dusts released from the closed divertor region in the inboard side of the torus just before the plasma termination. Small sized incandescent dusts move to the upper-left

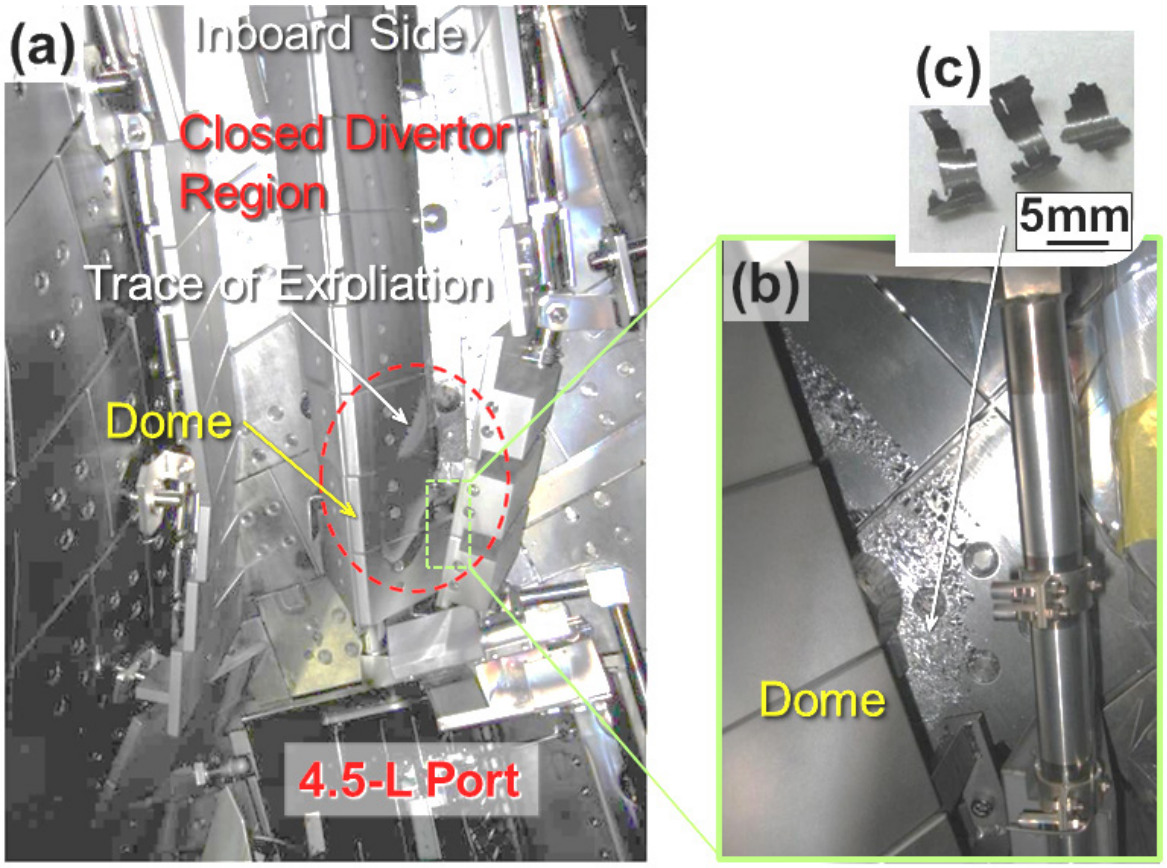

Figure 8. (a) A picture of the closed divertor region in the inboard side of the torus near a lower port (4.5-L) after the last experimental campaign in 2013. Some traces of exfoliation of the deposition layers were found on dome structures and the surface of a vacuum vessel in the inboard side of the torus. (b) An enlarged picture of the deposition layers in the closed divertor region directly faced to the divertor plates. (c) A picture of collected giant sized dusts which were exfoliated from deposition layers in the closed divertor region.

side in the images, which agree with the direction of the plasma flow along the magnetic field lines in a lower divertor leg. An intensive bright stripe was observed after 2859.8194s, which appeared from a positon in the closed divertor region (inboard side). From the above two observations with the cameras installed in 5-O and 4.5-U ports, the position of the dust source is identified as a closed divertor region in the inboard side of the torus near a lower port (4.5-L).

Abrupt increase in the emission of carbon ions was observed with moderate rise of the emission of iron ions just before the plasma termination [9, 13]. Stable plasma heating by ICRF was sustained by the end of the discharge. After the experimental campaign, the traces of exfoliation of mixed-material deposition layers were found on the surface of the vacuum vessel and the dome structures locating at the position where release of the dusts were observed (see figure 8). Partially exfoliated giant sized dusts (>1mm) were collected in the closed divertor region. It is a completely different condition from that in the original open divertor configuration in which the maximum dust radius collected inside the vacuum vessel was in the order of 100μm at the most [16]. The closed divertor configuration can enhance the accumulation of the deposition layers by physical and chemical sputtering from the divertor plates onto the surface directly faced to divertor plates

A Transmission Electron Microscope (TEM) analysis using a nano-geological diagnostic technique clarified that the exfoliated dusts are mainly composed of carbon-rich mixed materials which are easily exfoliated from brittle iron-rich layers formed in a part of the dusts [17, 18]. This analysis is consistent with the observations of the abrupt increase in the emission of carbon and iron ions just before the termination of the long pulse discharge. It is possible that carbon sputtered from

divertor plates during the long pulse discharges formed the carbon-rich mixed materials on the surface in the closed divertor region. The layers were exfoliated from the brittle iron-rich layers by formation of blistering in the layers, and/or by thermal distortion induced by heat load in the long pulse discharges. The exfoliated dusts could lead to the release of large amounts of dusts from the closed divertor region. It is possible that the large amounts of dusts including the carbon-rich layers penetrated into the main plasma, which caused impurity accumulation in the plasma [19], and also deteriorated the ICRF heating efficiency due to the shrink of the plasma by cooling down the peripheral plasma temperature, which were actually measured by Thomson scattering. It could finally lead to the radiation collapse in the long pulse discharge.

5. Dust transport simulation in the plasma for the long pulse discharges

Theoretical and computational modelling of dust dynamics in plasmas has been developed for this decade for understanding dust production and transport mechanism in fusion devices [20]. The study of dust transport in realistic axisymmetric tokamak plasma geometries became possible using a dust transport simulation code (DUSTT) [21]. In order to apply this code to non-axisymmetric plasma geometries such as LHD configurations, a dust tracking sub-program in the DUSTT code was implemented in a three-dimensional neutral particle transport simulation code (EIRENE) [22]. It enables dust transport simulation in fully three-dimensional geometries using the grid model for the EIRENE code. The simulation has found that the LHD peripheral plasma has a function to shield the main plasma against the dust penetration by the effect of the plasma flow (mainly by the ion drag force) in the divertor legs and the heat load onto the dusts in the ergodic layer [23]. It is also shown that the three-dimensional trajectories of the most of the dusts moving along the magnetic field lines in the peripheral plasma can be explained by the simulation, which indicates the validity of the simulation [11]. For detailed analysis of the dust shielding effect due to the peripheral plasma in the long pulse plasma discharges, carbon dust trajectories are calculated using the DUSTT code which is modified for the dust transport analysis in the LHD configurations. The code can calculate the time evolution of the force, heat, energy and charge balances in spherical shaped dusts in plasmas [24-26]. It is assumed that the dust is composed of a homogeneous material which can be used in future nuclear fusion reactors such as carbon, iron and tungsten, etc. The three-dimensional profiles of background plasma parameters (the plasma density and the ion/electron temperature, the plasma flow velocity and so on) are supplied by an edge plasma fluid code (EMC3) [27-29] coupled with the EIRENE code for

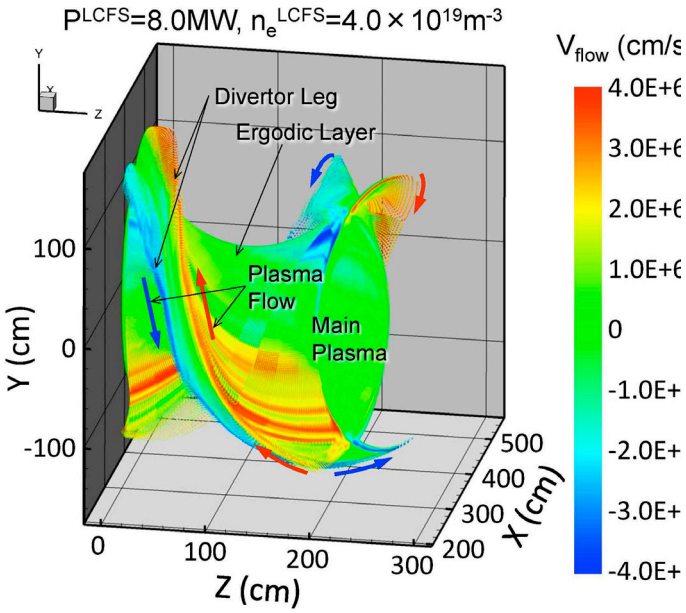

Figure 9. A perspective view of a three-dimensional profile of the plasma flow velocity parallel to magnetic field lines in the LHD peripheral plasma. It is calculated by the EMC3-EIRENE code under the condition where the plasma heating power and the plasma density at the LCFS are 8.0MW and 4.0×10^{19}m^{-3}, respectively. Red/blue colored dots in this figure indicate the plasma flow velocity which direction is clockwise/counterclockwise when it is looked from a vertically upper position (+Y side). It shows that the absolute plasma flow velocity in the divertor legs near divertor plates and that in the ergodic layer around the legs is as high as about 4.0×10^{6}cm/s.

the standard magnetic configuration (R_{ax}=3.60m). In the EMC3-EIRENE code, the heating power P^{LCFS} and the plasma density n_e^{LCFS} at the LCFS are necessary as initial input parameters for calculating the peripheral plasma parameter profiles.

As a typical example of the calculation of the EMC3-EIRENE code, a perspective view of the three-dimensional profile of the plasma flow velocity parallel to magnetic field lines (V_{flow}) in the LHD peripheral plasma is illustrated in figure 9, where the plasma heating power and the plasma density at the LCFS are set to 8.0MW and 4.0×10^{19}m^{-3}, respectively. It shows that high absolute plasma flow velocities $|V_{flow}|$ (~4.0×10^{6}cm/s) are formed in the divertor legs near divertor plates and in the ergodic layer around the legs.

Figure 10 (a) shows a perspective view of a three-dimensional model of a LHD plasma and the vacuum vessel for the closed divertor configuration with the vector plots of the plasma flow velocities in the peripheral plasma for analyzing dust trajectories in the long pulse discharge. In this simulation, the initial position of dusts is set to the surface on a dome structure in the lower closed divertor which position is identified as the main source of the dusts which released at the end of the ICRF heated long pulse discharge in the last experimental campaign. It is assumed that dusts purely consist of carbon with an initial temperature of 400K (a room temperature). The initial dust velocity is set to 5m/s, which is estimated as the most probable initial dust velocity from the analyses of the observations of the three-dimensional dust trajectories shown in figure 5. The injection angle of the dusts is set to the direction toward the plasma center. Figure 10 (b) gives the calculated trajectories of various sized dusts under the condition where the plasma heating power and the plasma density at the LCFS are 1.0MW and 1.0×10^{19}m^{-3}, respectively. This calculation condition corresponds to that in the long pulse plasma discharge in the last experimental campaign. The initial dust radius (r_{dust}) is changed from 1μm to 1mm, including giant sized dusts exfoliated from the deposition layers in the closed divertor region. It shows that the small sized dusts (r_{dust}≤4μm) are swept off by the effect of the plasma flow in a lower

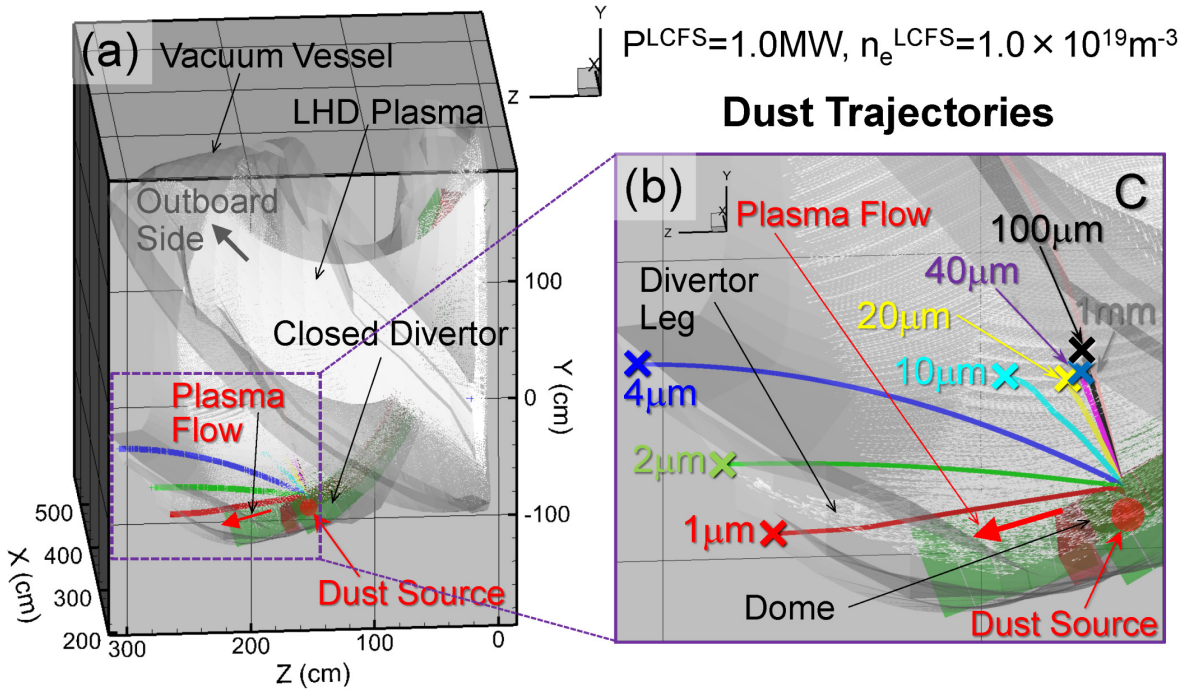

Figure 10. (a) A perspective view of a three-dimensional model of a LHD plasma and the vacuum vessel in a standard magnetic configuration (R_{ax}=3.60m) for the closed divertor configuration. The plasma flow velocities are indicated as vector plots (small white arrows). (b) An enlarged view of calculated carbon dust trajectories with various radii varying from 1μm to 1mm (colored lines). The position of the dust source is marked by a red circle. The direction of the representative plasma flow velocity in the divertor leg near the dust source is indicated as a thick red arrow. The positions where the dusts collide with the vacuum vessel or sublimated in the peipheral plasma are shown as colored crosses.

divertor leg.

The calculated small sized dust trajectories are consistent with the observations taken with the fast framing camera installed in the upper port (4.5-U) as shown in figure 11, which demonstrates that the small sized dusts approximately move along the magnetic field lines to the plasma flow directions in the lower divertor leg. The trajectories of the medium and giant sized dusts (r_{dust}≥10μm) stay near the dust source in the closed divertor region near the lower port, which is due to the large inertial effect of the dusts. It strongly suggests that the intensive bright stripe flown out from a position near the dust source, which was observed from the upper port (2nd, 3rd and 4th frames in figure 7), was caused by the penetration of the medium and/or giant sized dusts into the main plasma just before termination of the long pulse discharge.

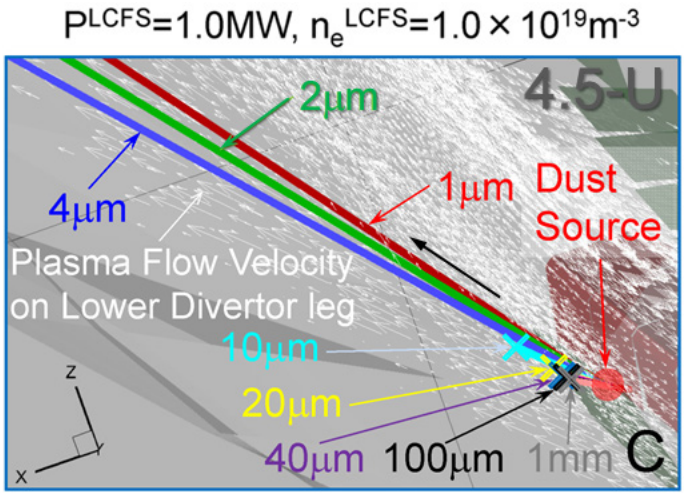

Figure 11. Calculations of the trajectories of various sized carbon dusts (1μm≤r_{dust}≤1mm) released from the position of the dust source in the closed divertor region, which are viewed from the position of the fast framing camera installed in an upper port (4.5-U). Small white arrows represent the direction of the plasma flow velocity on the lower divertor leg close to the dust source (red circle).

Figure 12 is the calculations of the time evolution of the temperature, mass and velocity of the various sized carbon dusts. It indicates that small sized dusts (r_{dust}≤4μm) are immediately heated up by the heat load in the divertor leg, and swept off by the effect of the plasma flow in the divertor leg at t~0.02s. Medium sized dusts (10μm≤r_{dust}≤100μm) penetrate the divertor leg and reach to the ergodic layer to heat up by the heat load in the ergodic layer at t~0.1s, which leads to sublimation of dusts with abrupt fall of the mass. The giant sized dust (r_{dust}=1mm) penetrates the ergodic layer and sublimates in the main plasma inside of the LCFS. The temperature of the dusts in the sublimation phase is determined by equilibrium of the energy balance mainly between the output power flux due to sublimation, radiation and the heat power load onto the dust by the plasma. The simulation indicates that control of the radius of dusts to less than about 1mm is indispensable in order to prevent the main plasma from penetration of dusts in the long pulse discharges.

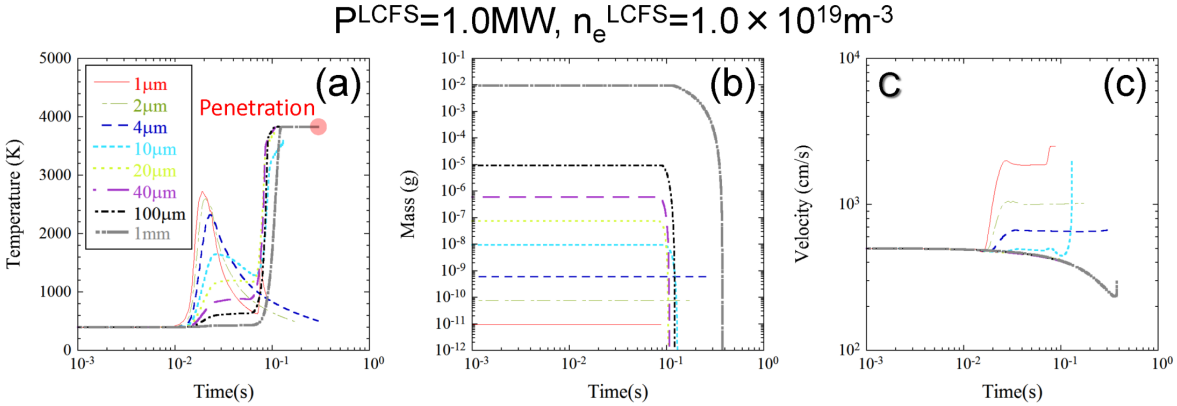

Figure 12. Time evolution of the temperature (a), mass (b) and velocity (c) of various sized carbon dusts calculated by the modified dust transport simulation code under the condition of a long pulse discharge in the last experimental campaign (P^{LCFS}=1.0MW and n_e^{LCFS}=1.0×10^{19}m^{-3}). A red circle in the temperature evolution indicates penetration of a dust into the main plasma.

6. The effect of high heating power operation on transport of heavy metal dusts

In addition to the simulation for carbon dust, transport of heavy metal (high Z) dusts such as iron and tungsten is also investigated using the modified dust transport simulation code. Enlarged view of the three-dimensional trajectories of spherical carbon, iron and tungsten dusts are presented in figure 13, where the calculation condition is same as that in figure 10 except for the plasma parameters at the LCFS. The plasma heating power and the plasma density at the LCFS are set to 4.0MW and 4.0×10^{19}m^{-3}, respectively. The heating power and the plasma density are typical ones in normal short pulse (several seconds) plasma discharges in the LHD. It shows that the heavy metal dusts tend to reach the ergodic layer and penetrate into the main plasma for medium and giant sized dusts compared to those for the carbon dusts. It looks that the sweeping effect of small sized dusts in the divertor leg weakens for heavy metal dusts. It is because the inertial effect of the heavy metal dusts has a function to keep the direction of the initial dust velocity against the effect of the plasma flow.

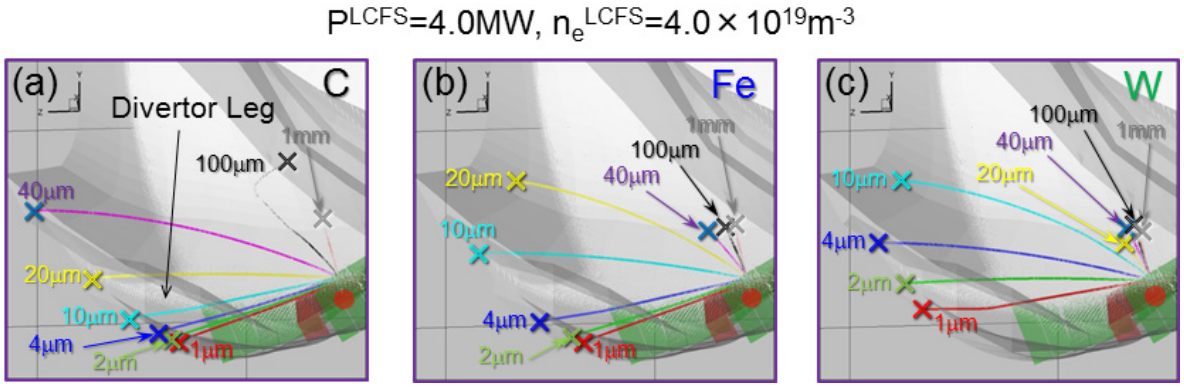

Figure 13. Enlarged views of the three-dimensional trajectories of (a) carbon, (b) iron and (c) tungsten dusts near the dust source (red circles) in a moderate plasma heating power case where the plasma heating power and the plasma density at the LCFS are 4.0MW and 4.0×10^{19}m^{-3}, respectively.

It is expected that higher temperature in the peripheral plasma in high heating power operation hinders the dusts from penetrating into the main plasma because the dusts can be effectively sublimated/evaporated by higher heat load by the peripheral plasma. The effect of the high heating power operation on transport of the dusts is investigated by calculating the dust trajectories under the condition where the plasma heating power P^{LCFS} is raised to 8.0MW (the plasma density P^{LCFS} is fixed to 4.0×10^{19}m^{-3}). The calculations of the three-dimensional trajectories of carbon, iron and tungsten dusts in this case are indicated in figure 14, showing that the small sized carbon dusts (r_{dust}<4μm) are sublimated near the dust source position, and that the trajectories of the small sized heavy metal dusts are bent to the lower side compared to those in the moderate plasma heating power case (figure 13).

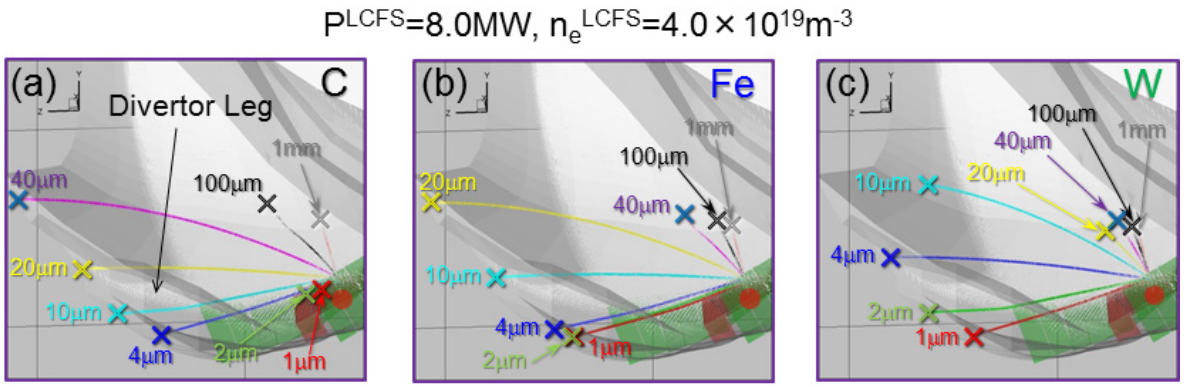

Figure 14. Enlarged views of the three-dimensional trajectories of (a) carbon, (b) iron and (c) tungsten dusts near the dust source (red circles) in a high heating power case where the plasma heating power and the plasma density at the LCFS are 8.0MW and 4.0×10^{19}m^{-3}, respectively.

This enhanced dust sweeping for high heating power operation is caused by the increased heating power onto the dusts and enhanced flow velocity due to the higher plasma temperature in the divertor leg. It strongly suggests that high heating power operation is effective to shield the main plasma from penetration of the small sized dusts released from the divertor region.

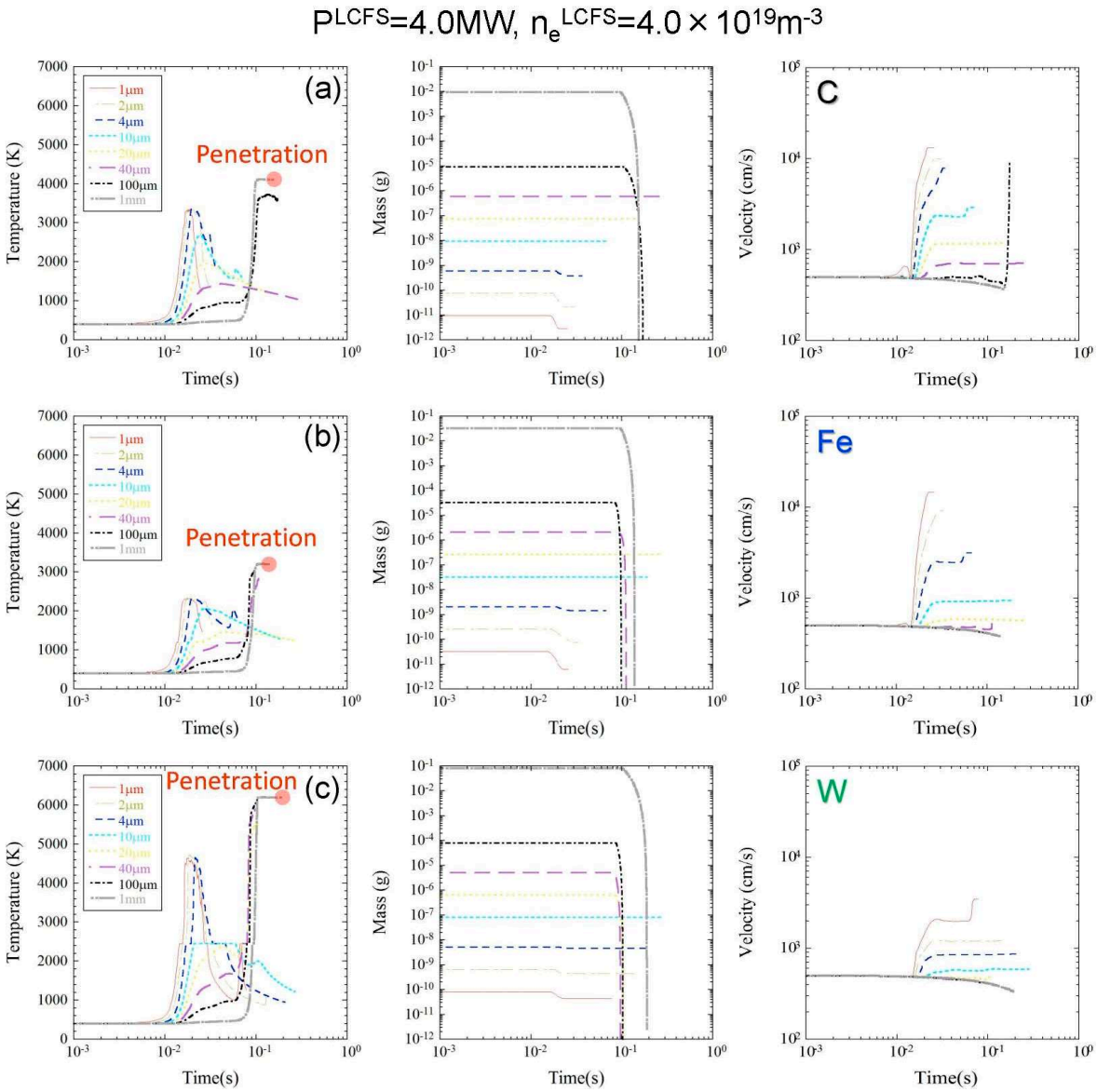

Figure 15. The time evolution of the temperature, mass and velocity of various sized carbon (a), iron (b) and tungsten (c) dusts, respectively, which radii range from 1.0μm to 1.0mm, calculated by the modified dust transport simulation code, in a moderate plasma heating power case (P^{LCFS}=4.0MW, $n_e{}^{LCFS}$=4.0×10^{19}m^{-3}). Red circles in temperature evolution indicate the penetration of dusts into the main plasma.

Figure 15 (a), (b) and (c) are the calculated time evolution of the temperature, mass and velocity of various sized carbon (a), iron (b) and tungsten (c) dusts, respectively, in the moderate heating power case (P^{LCFS}=4.0MW, $n_e{}^{LCFS}$=4.0×10^{19}m^{-3}). The giant sized dust (r_{dust} =1mm) penetrates into the main plasma and sublimates/evaporates there in all dust material cases. The time evolution indicate that the temperature of the small sized dusts immediately rises by the heat load in the divertor legs, and the dusts are accelerated by the effect of the plasma flow. Acceleration of the small sized carbon dusts is more observable than that of the iron and tungsten dusts due to the small internal effect of the carbon dusts. The acceleration weakens with the size and the atomic number of the dust materials because of the inertial effects of the dusts. In general, medium and giant sized dusts reach

the ergodic layer to be heated up to the sublimation/evaporation points in the ergodic layer or in the main plasma. The mass of the dusts abruptly drops after reaching the sublimation/boiling point of the materials. While the temperature of the carbon dusts smoothly rises to the equilibrium temperature at sublimation (~4325K), that of the iron and tungsten dusts has a plateau at the melting points (1200K and 2450K, respectively) in the middle of the temperature rise to the equilibrium temperature at the

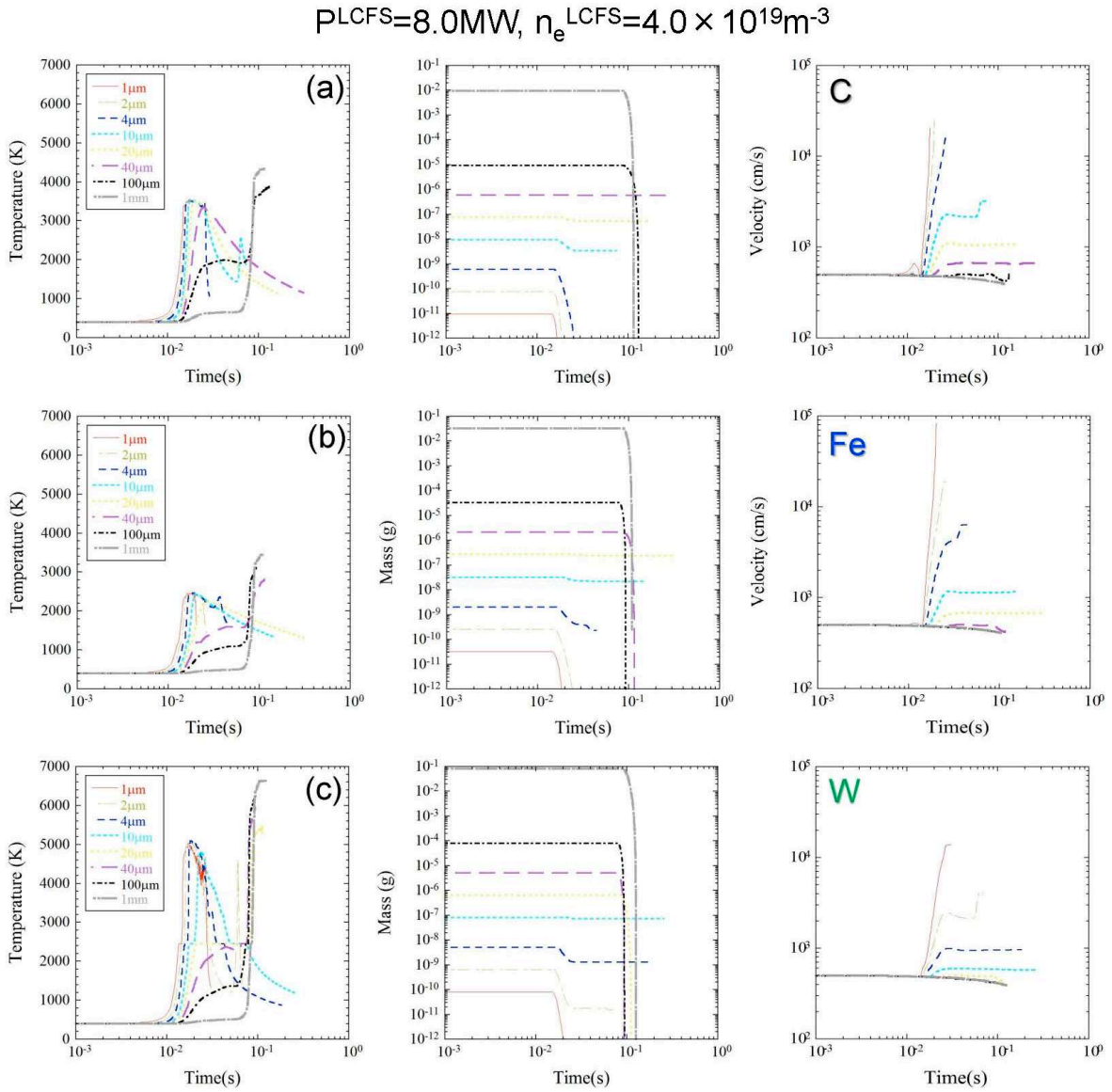

Figure 16. The time evolution of the temperature, mass and velocity of various sized carbon (a), iron (b) and tungsten (c) dust, which radii range from 1.0μm to 1.0mm, calculated by the modified dust transport simulation code, respectively, in a high plasma heating power case (P^{LCFS}=8.0MW, n_e^{LCFS}=4.0×10^{19}m^{-3}).

evaporation points (~3441K and ~6631K, respectively). In the moderate heating power case, the giant sized dust (r_{dust}=1.0mm) penetrate into the main plasma and sublimates/evaporates there in the all dust material cases.

The time evolution of the dust parameters for carbon (a), iron (b) and tungsten (c) dusts in the high heating power case (P^{LCFS}=8.0MW, n_e^{LCFS}=4.0×10^{19}m^{-3}) are given in figure 16. Temperature rise and acceleration of the small sized dusts are more clearly seen compared to those in the moderate plasma heating power case (figure 15), and drop of the mass of the medium and giant sized dusts at reaching the ergodic layer is more observable. In the high heating power case, the giant sized dust sublimates/evaporates in the ergodic layer in all dust material cases because of higher heat load onto

the dusts in the ergodic layer, which is different situations from those in the moderate heating power case.

For summarizing the dependence of the dust trajectories on the plasma heating power in the three different dust material cases, categorized plots showing the classification of the ends of the dust trajectories are shown in Figure 17, in which the ends of the trajectories of various sized dusts ($1\mu m \leq r_{dust} \leq 2mm$) are classified by three different marks under conditions where the plasma heating power at the LCFS is varied from 1MW to 8MW with a fixed plasma density condition at the LCFS of $n_e^{LCFS}=4.0\times10^{19}m^{-3}$. When a dust penetrates into the main plasma, a closed circle is plotted in the figure, and when it sublimates or evaporates in the ergodic layer, a gray circle is plotted. In the case where the dust is swept off in divertor legs, an open circle is plotted in the figure. It shows that high plasma heating power operation ($P^{LCFS}=8.0MW$) is effective to shield the main plasma from the penetration of giant sized dusts ($r_{dust}=1.0mm$) in all dust material cases. The small sized dusts are swept off by the effect of the enhanced plasma flow in the divertor legs, and the medium and giant sized dusts are sublimated/evaporated by higher heat load onto the dusts by the high temperature plasma in the ergodic layer. The categorized plot also proves that the giant sized tungsten dusts have a powerful penetration characteristic compared to that of the carbon and iron dusts because of the large inertial effect and the high boiling point. The simulation shows that giant sized carbon and tungsten dusts which radius is more than 1.6mm and 1.0mm respectively can penetrate into the main plasma even in the high plasma heating power case. Control of the size of tungsten dusts can be a critical issue for sustaining steady-state plasma discharge operation in future nuclear fusion reactors because of the large cooling rate of high-Z materials on plasmas.

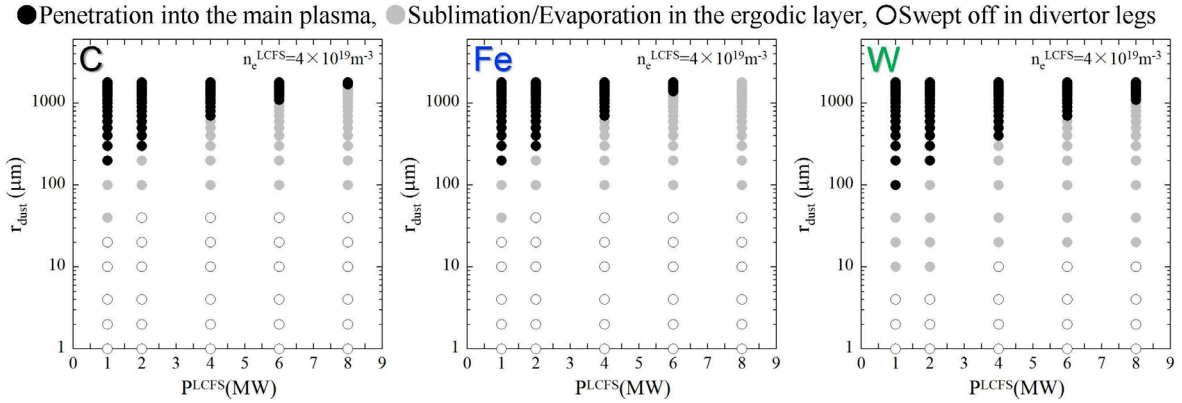

Figure 17. Categorized plots showing the ends of the calculated dust trajectories for carbon, iron and tungsten dusts under conditions where the plasma heating power at the LCFS is varied from 1MW to 8MW with a fixed plasma density at the LCFS of $4.0\times10^{19}m^{-3}$. It presents the ends of the trajectories of various sized dusts ($1\mu m \leq r_{dust} \leq 2mm$) which are classified by three different marks: solid circles (the dust penetrates into the main plasma), gray circles (the dust sublimates or evaporates in the ergodic layer) and open circle (the dust is swept off in divertor legs).

7. Summary

Observations of the three-dimensional dust trajectories with stereoscopic fast framing cameras in the LHD show that the trajectories of dusts locate in the peripheral plasma (ergodic layer and divertor legs). It also presents that the most of the dusts move along magnetic field lines and the moving direction corresponds to that of the plasma flow in the peripheral plasma. The time evolution of the observed dust velocity indicates that the most of dusts moves with acceleration and an initial dust velocity is estimated to be about 5m/s. Long pulse plasma discharges in the last experimental campaign in 2013 were often terminated with large amounts of dusts released from a closed divertor region near lower and upper ports with abrupt increase in the emission of carbon ions. The traces of exfoliated mixed-material deposition layers were found on the sites after the experimental campaign in the closed divertor region where is directly faced to divertor plates. In this region, some partially exfoliated giant sized dusts ($r_{dust}>1mm$) composed of carbon-rich mixed material layers with brittle

iron-rich layers formed in a part of the dusts were collected. Analyses using a modified dust transport simulation code present that small sized carbon dusts (r_{dust}≤4μm) released from the dust source position (closed divertor region near a lower port in the inboard side of the torus) are swept off by the effect of the plasma flow in the divertor leg, and the medium sized dusts (10μm≤r_{dust}≤100μm) reach the ergodic layer and sublimate there by the heat load onto the dusts due to the plasma in the ergodic layer. The giant sized dust (r_{dust}=1mm) penetrates into the main plasma. It indicates that the control of the radius of dusts to less than 1mm is indispensable for preventing the main plasma from dust penetration for the long pulse plasma discharges. Dust transport simulations including heavy metal (iron and tungsten) dusts demonstrate that high plasma heating power operation is effective for preventing dusts from penetrating into the main plasma by an enhanced plasma flow effect in the divertor leg and high heat load onto the dusts in the ergodic layer. It also shows that tungsten dusts have a powerful penetration characteristic into the main plasma compared to that of carbon and iron dusts because of the large inertial effect and the high boiling point. Giant sized carbon (r_{dust}>1.6mm) and tungsten dusts (r_{dust} >1.0mm) penetrate into the main plasma even in the high plasma heating power case in the LHD.

Acknowledgements

This work is financially supported by NIFSULPP015 and is performed with the support and under the auspices of the NIFS Collaboration Research program (NIFS12KNXN236). It is performed by NIFS/NINS under the project of Formation of International Scientific Base and Network with an international collaboration research framework between NIFS and CIEMAT in Spain.

References

[1] Krasheninnikov S. I. et al 2008 *Plasma Phys. Control. Fusion* **50** 124054

[2] Hong S. et al 2010 *Nucl. Fusion* **50** 035002

[3] Temmerman G. et al 2010 *Nucl. Fusion* **50** 105012

[4] Rudakov D. L. et al 2009 *Nucl. Fusion* **49** 085022

[5] Ratynskaia S. et al 2011 *Plasma Phys. Control. Fusion* **53** 074009

[6] Federici G. et al 2001 *Nucl. Fusion* **41** 12R

[7] Rosanvallon S. et al 2009 J. *Nucl. Mater.* **390-391** 57

[8] Saito K. et al 2007 *J. Nucl. Mater.* **363–365** 1323

[9] Kasahara H. et al "Progress of high-performance steady-state plasma and critical PWI issue in the LHD" EX/7-3, paper presented at *25th IAEA Int. Conf. on Fusion Energy St Petersburg 2014.*

[10] Komori A. et al 2010 *Fusion Sci. and Technol.* **58**, 1

[11] Shoji M. et al "Analysis of the three-dimensional trajectories of dusts observed with a stereoscopic fast framing camera in the large helical device" *21st Int. Conf. on Plasma Surface Interactions (Kanazawa, Japan, 2014), J. Nucl. Mater.* accepted

[12] Mutoh T. et al 2003 *J. Nucl. Mater.* **313–316** 1131

[13] Shoji M. et al "Measurements of plasma termination in ICRF heated long pulse discharges with fast framing cameras in the large helical device" P4-15, *24th Int. Toki Conf. (Toki, Gifu, Japan, 2014), J. Plasma Fusion Res.* accepted

[14] Seki T. et al et al "ICRF Heating Experiment using the Faraday Shield Less Antenna and New High Power Antenna in LHD" FIP/P5-3, paper presented at *25th IAEA Int. Conf. on Fusion Energy St Petersburg 2014.*

[15] Morisaki T. et al 2012 First results of closed helical divertor experiment in LHD *Proc. 24th Int. Conf. on Fusion Energy (San Diego, USA 2012)* (Vienna: IAEA) paper EX/P5-29 andhttp://www-naweb.iaea.org/napc/physics/FEC/FEC2012/html/fec12.htm

[16] Koga K. et al 2009 *Plasma Fusion Res.* **4** 034

[17] Tokitani M. et al 2013 *J. Nucl. Mater.* **438** S818

[18] Tokitani M. et al 2014 Plasma wall interaction in long pulse helium discharge in LHD ~ Microscopic modification of wall surface and its impact on particle balance and impurity generation ~ *21st Int. Conf. on Plasma Surface Interactions (Kanazawa, Japan, 2014), J. Nucl. Mater.* Submitted

[19] Sudo S. et al 2013 *Plasma Phys. Control. Fusion* **55** 095014

[20] Krasheninnikov S. I. et al 2004 *Phys. Plasmas* **11** 3142

[21] Pigarov A. Y. et al 2005 *Phys. Plasmas* **12** 122508

[22] Reiter D. et al 2005 *Fusion Sci. Technol.* **47** 172

[23] Shoji M. et al 2014 *Plasma Fusion Res.* **9** 3403132

[24] Pigarov A. Y. et al 2007 *J. Nucl. Mater.* **363-365** 216

[25] Smirnov R. D. et al 2007 *Plasma Phys. Control. Fusion* **49** 347

[26] Tanaka Y. et al 2011 *J. Nucl. Mater.* **415** S1106

[27] Feng Y. et al 2002 *Plasma Phys. Control. Fusion* **44** 611

[28] Kobayashi M. et al 2010 *Fusion Sci. and Technol.* **58** 220

[29] Kawamura G. et al 2014 *Contrib. Plasma Phys.* **54** 437